JOURNAL OF CATALYSIS 157, 162–178 (1995)

Molecular Aspects in Syn-Gas Production: The CO_2-Reforming Reaction Case

L. Basini[1] and D. Sanfilippo

Snamprogetti S.p.A. Research Laboratories, Via Maritano 26, 20097 San Donato Milanese (MI), Italy

Received August 9, 1994; revised April 27, 1995; accepted May 22, 1995

CO_2-reforming reactions have been studied in a plug-flow reactor with catalysts containing less than a monolayer of Rh, Ru, or Ir deposited from tetrametallic dodecacarbonyl clusters onto low surface area polycrystalline α-Al_2O_3, MgO, CeO_2, La_2O_3, and TiO_2. The catalytic reactions are studied in conditions at which the carbon formation quickly deactivates Ni-based catalysts but does not deactivate noble metal based materials. Diffuse-reflectance-infrared-Fourier-transform (DRIFT) spectroscopy and mass spectrometry experiments inside a high-temperature high-pressure (HTHP) chamber have cast light on molecular aspects of the CO_2-reforming reaction which have been embodied in a reaction mechanism. The formation of highly reactive oxidic species from the dissociation of CO_2 is showed, and their role in inhibiting the production of large carbon aggregates is discussed. © 1995 Academic Press, Inc.

INTRODUCTION

Syn-gas production technology plays a central role in petrochemistry. It is a demanding technology which absorbs the 50–70% of the investment and energy consumption costs of the processes in which the syn-gas is an intermediate product. Improvements are difficult to achieve due to the drastic reaction conditions and to the delicate and complex interactions among process schemes, reactor design and materials, reaction conditions, and catalyst activity. Many reasons, such as the possibility of producing clean fuels from natural gas and the exploitation of many of the results of the thoroughly investigated "C1 chemistry," push for the reduction of syn-gas production costs (1).

The widespead production processes, namely, (a) steam-reforming, (b) autothermal reforming, (c) noncatalytic partial oxidation, and (d) combined reforming, have been reviewed in Refs. (2–6) and are the object of several patents.

In noncatalytic partial oxidation, mixtures of oxygen, steam, and hydrocarbons (often heavy oil or feedstocks with high concentrations of impurities such as olefins and sulphur-containing compounds) are flowed through the reactor at pressures up to 13.5 MPa and temperatures between 1350 and 1600°C. The other commercial catalytic processes utilize catalysts constituted by nickel (15–25 wt%) supported by $MgAl_2O_4$ oxides, and usually the exit temperature from the reactors is below 1000°C and the pressure is below 4.5 MPa.

Recently renewed attention in both academic and industrial research has been focused on catalytic partial oxidation [1] (hereafter referred to as CPO) and on the CO_2-reforming reaction [2] (7–22).

$$CH_4 + 1/2\,O_2 \rightarrow CO + 2\,H_2 \qquad \Delta H^\circ_{298\,K} = -38\ \text{kJ/mole} \quad [1]$$

$$CO_2 + CH_4 \rightarrow 2\,CO + 2\,H_2 \qquad \Delta H^\circ_{298\,K} = 247\ \text{kJ/mole} \quad [2]$$

Two themes in particular are under investigaton: (i) the development of new catalysts that are inactive towards the carbon formation reactons

$$2\,CO \rightarrow C + CO_2 \qquad \Delta H^\circ_{298\,K} = -172.54\ \text{kJ/mole} \quad [3]$$

$$CH_4 \rightarrow C + 2\,H_2 \qquad \Delta H^\circ_{298\,K} = 74.91\ \text{kJ/mole}, \quad [4]$$

(ii) the possibility of producing syn-gas with CPO reactions performed in ultrahigh space velocity conditions (UHSV) at residence times inside the catalytic beds between 10^{-2} and 10^{-4} s.

Many of the energetic consumption and investment costs in the syn-gas producton technologies are related to the necessity of inhibiting carbon formation reactions [3 and 4]. These reactions are avoided by feeding the reactors with reactant mixtures in which high values of the O_2/C and/or H_2O/C molar ratios (typically $O_2/C = 0.65$ vol/vol for the autothermal and combined reforming, and $H_2O/C > 2.5$ vol/vol for the steam reforming) are main-

[1] To whom correspondence should be addressed.

0021-9517/95 $12.00

tained. Rostrup-Nielsen *et al.* (22–26), Alstrup (27), and Gadalla *et al.* (28–30) have discussed these problems in relation to the steam and CO_2-reforming reactions catalyzed by Ni-based materials; the reactivity of noble metal based materials is discussed by different authors and some of their works are reported in Refs. (31–37). The proposed solutions consider: (i) the possibility of adopting noble metal based catalysts; (ii) a sulphur passivated reforming process in which the Ni large crystalline sites, which are the major factor responsible for carbon nucleation, are sulphur-poisoned by adding a low percentage of sulphur to the process feed (27); and (iii) the stabilization in reaction conditions of fine Ni clusters formed and stablized from thermal treatments of periclase solutions of NiO–MgO (28–30).

Major research groups in petrochemical industrial environments and have also been active in these stimulating fields, and traces of their work can be found in a few scientific publications (19–21, 38) and many recent patents (39–51).

This work discusses the surface chemistry of noble metal clusters and their catalytic properties in the CO_2-reforming reactions. These have been investigated by feeding with a $CO_2 + CH_4$ mixture ($CO_2/CH_4 = 1/1$ vol/vol) a laboratory-scale plug flow reactor or by flowing various gaseous atmospheres through a high-temperature high-pressure (HTHP) chamber for DRIFT spectroscopy. The chamber has been linked, through a pressure reduction sampling system, to a quadrupole mass spectrometer.

The DRIFT and mass spectrometry experments are part of an extensive research program devoted to the HTHP chemistry of small aggregates and/or monoatomic species of Rh, Ru, and Ir at the surfaces of low-surface area polycrystalline oxides. The research program is more particularly devoted to investigating the surface chemistry produced during CO hydrogenation, CO_2 hydrogenation, and syn-gas production reactions. The main steps of 14 experimental sequences, on which the research program is based, are represented in Fig. 1. We have discussed the results of experiments 1–8 previously (53, 54); here we will report and discuss the results of experiments 9 and 10, while the results of experiments 11–14, will be commented on in a following article devoted to the CPO reaction mechanisms.

The experiments discussed here, gave indications of the high mobility ≡ reactivity of the noble metal species and other elements that have suggested the description of a cyclic reaction mechanism for CO_2 reforming. The reaction intermediates include hydridocarbonyl clusters and highly reactive oxidic species formed by the breaking of one of the two CO_2 bonds. These oxidic species react with the carbon atoms produced with the CH_4 surface decomposition to originate CO. The formation of highly reactive oxidic species is considered responsible for the inhibition of large carbon aggregates which, in analogous conditions, deactivate the Ni-based catalysts.

EXPERIMENTAL

Sample Preparations

The Rh- (1 wt%) and Ru- (1 wt%) containing samples were prepared in a N_2 environment, by dropping an anhydrous THF solution of $Rh_4(CO)_{12}$ or $Ru_3(CO)_{12}$ into a slurry of the supports in the same solvent. δ-Al_2O_3 (Snamprogetti, surface area 95 m^2/g) and MgO polycrystalline samples (Fluka, surface area 65 m^2/g) were used as supports. After 3 h the solids were filtered and dried under vacuum at 25°C.

Samples containing low loading of Rh, Ru, and Ir (0.1–0.25 wt%) were also prepared with the same procedure by using the same clusters of Rh, Ru, and $Ir_4(CO)_{12}$. High-purity low surface area oxides (La_2O_3, TiO_2, and CeO_2, supplied by Johnson Matthey, 99.99%, and α-Al2O3 and MgO, supplied by Aldrich, 99,999%) were used in these cases. The oxides were purchased under N_2 to avoid interaction with moisture and CO_2. Their purity and crystalline structure were checked with opical emission arc spectroscopy and XRD analysis, while their surface area (below 10 m^2/g) was measured with the BET method. The reactivity of each sample was studied with the laboratory equipment described in the following. Four Rh/α-Al_2O_3, Rh/MgO, Rh/CeO_2, and Ir/α-Al_2O_3 samples, with low loadings of noble metals (0.1–0.25 wt%), were also studied with DRIFT and mass spectrometry experiments in a HTHP chamber. In these cases a dry box was used to load the samples into the chamber to avoid CO_2 and H_2O chemisorption from the environment.

A Ni/Al_2O_3 sample (Ni 15 wt%) was prepared by impregnating, with the incipient wetness method, γ-Al_2O_3 (surface area 137 m^2/g, pore volume 0.97 ml/g, medium pore diameter 180 Å) with an aqueous solution of $Ni(NO_3)_2 \cdot 6H_2O$. After a dehydration step at 120°C for 12 h, the sample was calcined at 1000°C for 3 h.

DRIFT and Mass Spectrometry Experiments

The HTHP chamber allows the collection of DRIFT and mass spectra in flowing gaseous atmospheres between 25 and 750°C at pressures between 0.1 and 5 MPa. The powdered polycrystalline materials (20–60 mg) were placed inside the chamber onto a porous fritted tungsten disk that could be heated up to 900°C and permitted the flow of the gaseous atmospheres through the samples. Two water-cooled ZnSe windows allowed the incident IR radiation to reach the samples and the diffuse-reflected radiation to be collected into a MCT detector. Light absorption phenomena in the gaseous phase were modeled with the Lambert–Beer treatment while those at the surfaces were

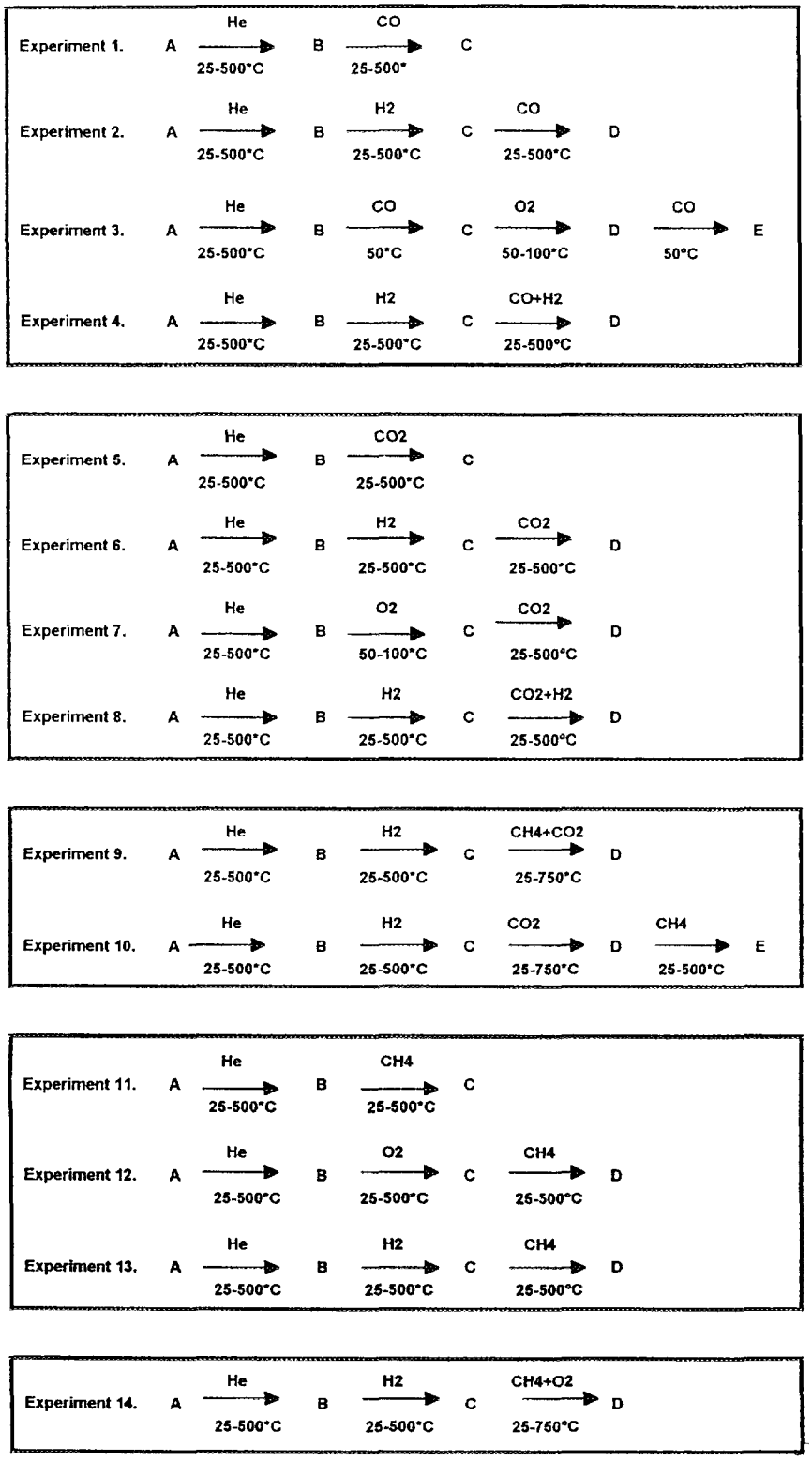

FIG. 1. Scheme of the experimental sequences performed to investigate the HTHP chemistry of the Rh and Ir clusters at the surfaces of MgO, α-Al_2O_3, and CeO_2.

modeled with the Kubelka–Munk equations. A chromel–alumel thermocouple was inserted into the powdered sample and used both to measure its temperature and to control the heating power. The reactant gases were flowed through the powdered catalysts into the output line. The output flow composition was monitored with a quadrupole mass spectrometer (UTI 1-300 a.m.u.) which was connected to the HTHP cell through a pressure reducton sampling system. DRIFT spectra were recorded at a resolution of 4 cm^{-1} with a Nicolet 20SXC spectrometer. Mass spectra were recorded both with repeated scans between 1 and 60 a.m.u. and with a selected peak monitoring with time and/or with temperature. High purity gases were flowed through the samples (Strem electronic grade). In some of the expermental steps, the purity of the CH_4, H_2, and He streams was critical and these gases were further purified with OM-1 filters (Supelco, Li, and Co compounds supported on resins which react with O_2, H_2O, CO, and CO_2 impurities). Reactant flows were measured and regulated with a multi-gas-flow controller system (147 C MKS) equipped with four mass flow meters. Flow rates measured at the entrance of the HTHP cell were maintained between 30 and 60 ml/min. The heating and cooling cycles were performed in several steps at a rate of 60°C/min; at each step the temperature was equilibrated for 5 min before the collection of the DRIFT spectra.

Laser-Raman Analysis

A laser-Raman spectrometer (Dilor triple monochromator spectrometer) equipped with a multichannel detector with 512 diodes (Omars) was used to record the spectra at point **A** of the experimental sequences. Due to the low concentration of the noble metal only the Ir/Al_2O_3 sample produced detectable Raman signals. In this case the spectra were achieved in a backscattering configuration with a slitwidth of 80 μm and with microscope sampling.

High-Resolution Electron Microscopy (HRTEM)

These measurements were performed on CeO_2 and Rh/CeO_2 powders (Rh 0.1 wt%) collected on a holey carbon film supported on a copper grid. The transmission electron microscope was a Jeol 2000EX instrument, equipped with a top entry stage (2.5 Å point resolution).

Laboratory Scale Reactor for CO2 Reforming Reactions

The CO2 reforming reactions were carried out in a tubular quartz plug-flow (PF) reactor with an internal diameter of 10 mm. The reactor was placed in an oven. A quartz thermowell with an external diameter of 3 mm was placed in the center of the reactor through the catalyst bed, which was 10 mm in height. The catalyst particles (500 mg of 0.3–0.5 mm fragments) were inserted into the annular zone (3.5 mm thick) between the thermocouple well and the internal wall of the reactor. Reactants (CH_4, CO_2, H_2, N_2) were supplied from cylinders into different lines, each equipped with a mass flow meter and a mass flow controller. The catalysts were pretreated with a H_2/N_2 mixture 1/1 (vol/vol) up to 500°C. The activity tests with a $CH_4 + CO_2$ gaseous mixture (CH_4/CO_2 = 1/1 vol/vol) were performed at 1.5 atm during thermal cycles between 25 and 750°C. The axial temperature gradient was 25°C at 750°C. The output line composition was monitored by gaschromatography with both TCD and flame detectors.

RESULTS

Morphological HRTEM Analysis of the CEO_2 and Rh/CeO_2 Samples

The HRTEM images were collected to investigate the formation of Rh clusters at the surface of CeO_2. The images obtained at low magnification showed that the CeO_2 and the Rh/CeO_2 powders (Rh 0.1–0.5 wt%) contained a large amount of hexagonal microcrystals with few kink and step defects. The high-resolution images of the hexagonal crystals showed the presence of fringes 3.1 Å apart, corresponding to the interplanar spacing of the (111) faces of Cerianite, which has a cubic structure belonging to the *Fm3m* space group (Fig. 2). The same images were also obtained with HRTEM analysis of Rh/CeO_2 treated in a flowing H_2 stream at 500°C. The formation of Rh aggregates was never detected, indicating that monometallic and/or small metal clusters with diameter <1 nm were formed at the CeO_2 surfaces.

DRIFT and Laser-Raman Analysis of the Freshly Prepared Samples

The spectra of the Rh-containing samples, recorded at point **A** of the experimental sequences, indicated that the monometallic $Rh^I(CO)_2$ complex ($\nu C = O$ at 2085 and 2008 cm^{-1} over MgO, $\nu C = O$ at 2090 and 2010 cm^{-1} over α-A_2O_3, $\nu C = O$ at 2095 and 2010 cm^{-1} over CeO_2) was the prevailing species formed at the surfaces. Other species were also detected in minor amounts at the surfaces of CeO_2; this was inferred from the observation of a carbonyl stretching band at 2110 cm^{-1}, assigned to a carbonyl group bonded to a Rh atom in an oxidation state higher than +1 (53). Strong absorptions at 1237 and 1160 cm^{-1} were also detected in the spectra of the Rh/CeO_2 sample and assigned to vibration of carboxylate species (55). The infrared and laser-Raman spectra of the Ir/α-A_2O_3 (the only sample that produced detectable Raman signals) showed that the chemisorption of $Ir_4(CO)_{12}$ produced $HIr_4(CO)_{11}^-$ species (56) (IR peaks at 2020 and 1730 cm^{-1}, Raman shifts at 2110, 2035, 2010, and 2001 cm^{-1}).

Activity Tests in the PFR Reactor

Four catalysts containing 1 wt% of Rh or Ru chemisorbed on δ-Al_2O_3 and MgO were reduced for 3 h at 500°C

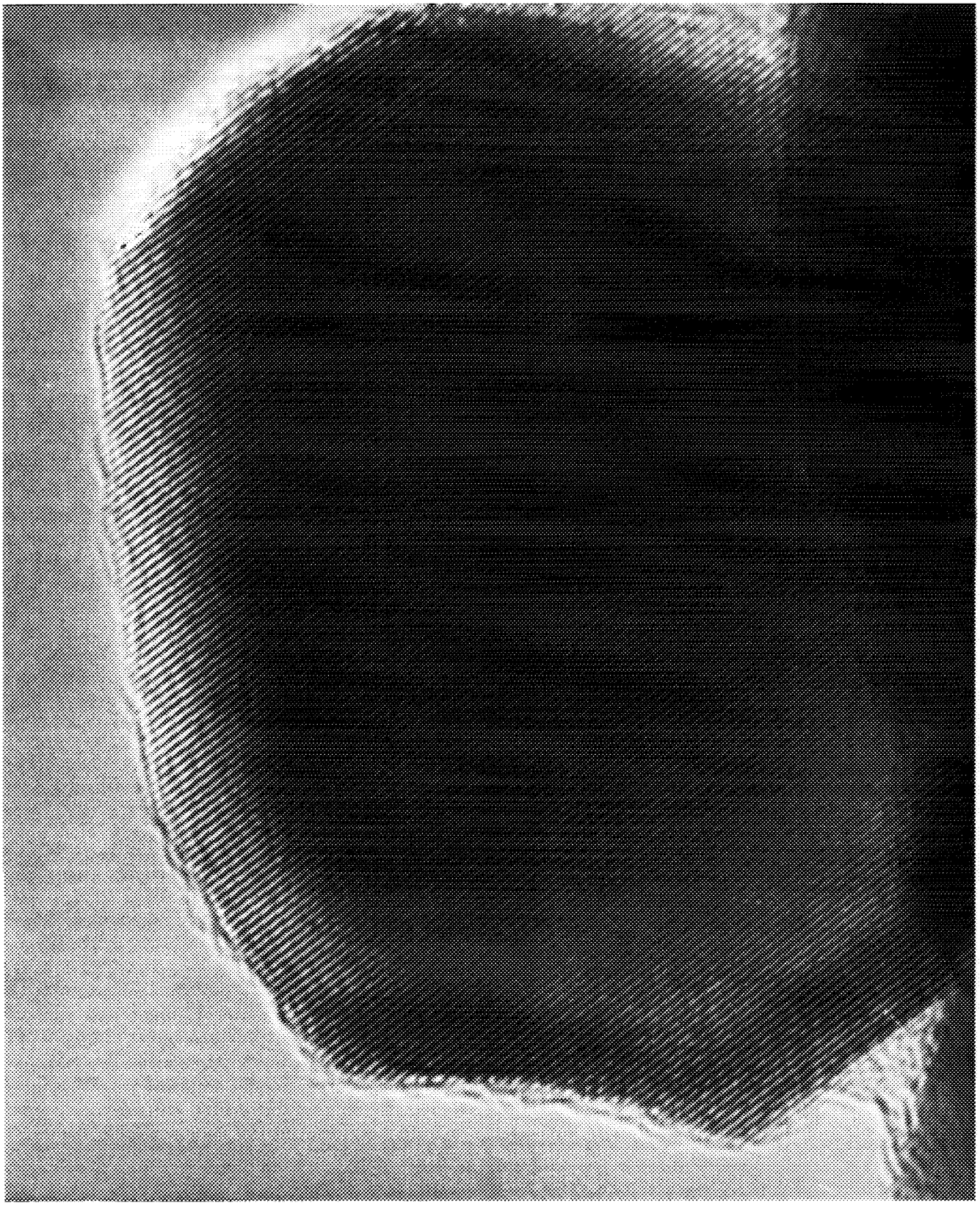

FIG. 2. HRTEM image of a Rh/CeO_2 crystal after reduction at 500°C under H_2 atmosphere (1 cm = 1.625 nm).

TABLE 1

Highest Turnover Frequency Values Measured during the CO_2 Reforming Experiment at 750°C

	$Rh/\alpha\text{-}Al_2O_3$	Rh/MgO	Rh/CeO_2	Rh/La_2O_3	Rh/TiO_2	$Ru/\alpha\text{-}Al_2O_3$	Ru/La_2O_3	$Ir/\alpha\text{-}Al_2O_3$
TF CH_4 (s^{-1})	5.02	1.04	2.82	4.01	0.74	1.05	4.05	1.00
TF CO_2 (s^{-1})	5.08	1.06	3.04	4.06	0.85	1.06	4.07	1.01
GHSV (h^{-1})	11000	3000	11000	11000	3000	3000	8100	3000
Support surface area (m^2/g)	4	6	5	8	8	4	5	4

in a 1/1 (vol/vol) $H_2 + N_2$ flowing atmosphere. The reduced samples were made to interact at 0.1 MPa at temperatures between 25 and 750°C with a gaseous mixture of 1/1 (vol/vol) $CH_4 + CO_2$. The four samples showed very similar reactivity at contact times between 7.2 and 1.2 s (GHSV = 500–3000 h^{-1}). The equilibrium concentrations for the CO_2-reforming [2] and water–gas shift [5] reactions were closely approached in the whole temperature range investigated.

$$CO + H_2O \rightarrow CO_2 + H_2 \quad \Delta H^\circ_{298\,K} = -41.16 \text{ kJ/mol} \qquad [5]$$

To appreciate the reactivity differences produced when Rh, Ru, or Ir were grafted on different supports, and to estimate the turnover frequency (TF) values of the catalytic sites, we reduced the contact times to 0.33 s (GHSV = 11000 h^{-1}) and prepared samples with low metal loadings (Rh = 0.1 wt%, Ru = 0.5 wt%, Ir = 0.25 wt%). The TF values were estimated by considering that each noble metal atom was exposed to the reactant mixture and was able to produce syn-gas. This assumption is based on (a) the HRTEM, DRIFT, and laser-Raman spectral analyses, which indicated that only monoatomic or small cluster species are formed on the freshly prepared materials, and b) the measure of the percentage of the exposed atoms which resulted between 90–100%. The percentage of the exposed metal atoms was measured with CO and H_2 selective chemisorption experiments performed on samples previously heated in He flow at 500°C and assuming that each one of the exposed Rh, Ru, or Ir atoms was able to coordinate one H_2 molecule or two carbonyl groups.

The maximum values of the turnover frequencies (TF) achieved with catalysts containing Rh, Ru, or Ir deposited on low surface area oxides (α-Al_2O_3, MgO, CeO_2, La_2O_3, and TiO_2 with surface areas $<10\ m^2/g$), are reported Table 1. These TF values, calculated for conditions close to the thermodynamic equilibrium, represent overall reaction rates. However, in many cases, the TF for the Rh- and Ru-containing materials are higher than the values reported in the literature (0.65–2.7 s^{-1}, see Refs. (2, 19)), measured under kinetic control and under conditions at which the carbon formation reactions were inhibited by using $CO_2/CH_4 \gg 1$ and by introducing H_2 in the feed gas.

The reactant conversions between 300 and 800°C, obtained with a catalyst containing 0.1 wt% of Rh deposited on La_2O_3, are reported in Fig. 3. In the same figure the experimental values are compared with the calculated thermodynamic values (determined with the Levenberg–Marquard algorithm). The catalyst activity can be expressed, according to industrial practice, with a measure of the "approach to equilibrium" defined with the temperature difference (ΔT),

$$(\Delta T) = T(Q_R) - T(\text{exit}), \qquad [6]$$

where $T(Q_R)$ is the temperature at which the quotient Q_R calculated from the product gas is equal to the equilibrium constant K_p, and T(exit) is the temperature measured at the exit of the catalyst bed (2). In the temperature range considered, between 300 and 400°C, we measured ΔT values below 3°C. This low value is a further indication of the high catalyst activity. We underline that during the reactivity tests of 100 h at 750°C only the Rh/La_2O_3 and Rh/CeO_2 materials did not show any deactivation process. The maximum TF values of the other catalysts were reduced by 10–15% during the first 50 h of reaction and remained unchanged for the following 50 h. The reactivity of the Rh/TiO_2 sample, in which strong metal support interactions occur, is very poor in comparison with the one observed with the other materials. A detailed investigation of the nature of the deactivation phenomena was not performed. However, we point out that the atomic absorption analysis of the exhausted materials revealed amounts of carbon below 0.01 wt%.

The CO_2-reforming reactions were also conducted with a Ni/Al_2O_3 (Ni 15 wt%) catalyst. This was initially reduced in $H_2 + N_2$ flow (H_2/N_2 = 1/1 vol/vol) at 700°C for 4 h and subsequently was made to interact with the $CO_2 + CH_4$ mixture. This caused the production of large carbon aggregates which completely filled the catalytic bed and occluded the reactor in a few seconds. As reported in the literature (2, 19), an analogous catalyst was not deactivated

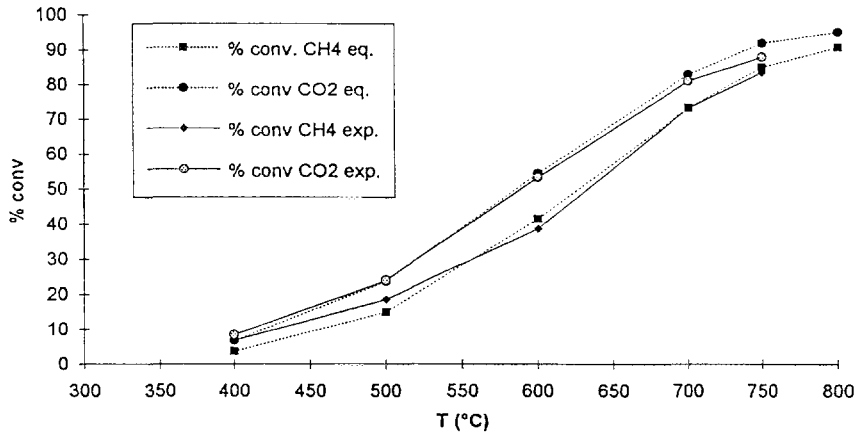

FIG. 3. Experimental and thermodynamic values for the CH_4 and CO_2 conversions between 400 and 750°C; the experimental values have been obtained with a Rh/La_2O_3 catalyst (Rh 0.1 wt%) at GHSV = 10,000 h^{-1}.

if reactant mixtures of $CO_2/CH_4/H_2$ = 16/4/1.5 (vol/vol) were used to feed the reactor.

DRIFT and Mass Spectrometric Experiments

The spectroscopic and spectrometric experiments 9 and 10 were performed on the Rh/MgO (Rh 0.1 wt%), Rh/α-Al_2O_3 (Rh 0.1 wt%), Rh/CeO_2 (Rh 0.1 wt%), and Ir/α-Al_2O_3 (Ir 0.25 wt%) samples, the reactivity features of which were previously studied in experiments 1–8.

Experiment 9

This experiment encompasses three sequential thermal treatments (see Fig. 1). The first heating was in a He flow, between 25 and 500°C, the second in a H_2 flow between 25 and 500°C, and the third between 25 and 750°C in a CO_2 + CH_4 flowing atmosphere (CH_4/CO_2 = 1/1 v/v, P_{tot} = 1.2 atm).

The reactivity of the Rh and Ir species formed in the freshly prepared samples during the thermal treatments in He (step A → B) and H_2 (step B → C), was reported previously (53, 54). The description of the third step of experiment 9 is given below in separate points for each examined sample.

Rh/MgO. Carbonyl absorption bands were formed at 300°C and at higher temperatures, in a flowing CO_2 + CH_4 atmosphere (Fig. 4). However, one peak at 2000 cm^{-1} (see Fig. 4B and Table 2) was also produced at 200°C by switching from a CO_2 + CH_4 flow to an He flow. This "low temperature" band disappeared again by reintroducing the CO_2 + CH_4 mixture in the HTHP cell. These effects were completely reversible and were reproduced several times. At higher temperatures between 300 and 400°C carbonyl bands were formed and stabilized both in flowing He and in flowing CO_2 + CH_4 atmospheres. However, in an inert atmosphere, the bands were reduced in intensity and shifted downward 10–20 cm^{-1}. Between 500 and 750°C a broad band at 1720 cm^{-1} was also shown in the spectra (Figs. 4E and 4F). The band, which was gradually reduced during the cooling cycle, is tentatively assigned to a CO stretching of a bidentate CO_3^- group (46). After cooling to 25°C, a 5-min CO pulse was introduced into the cell; this

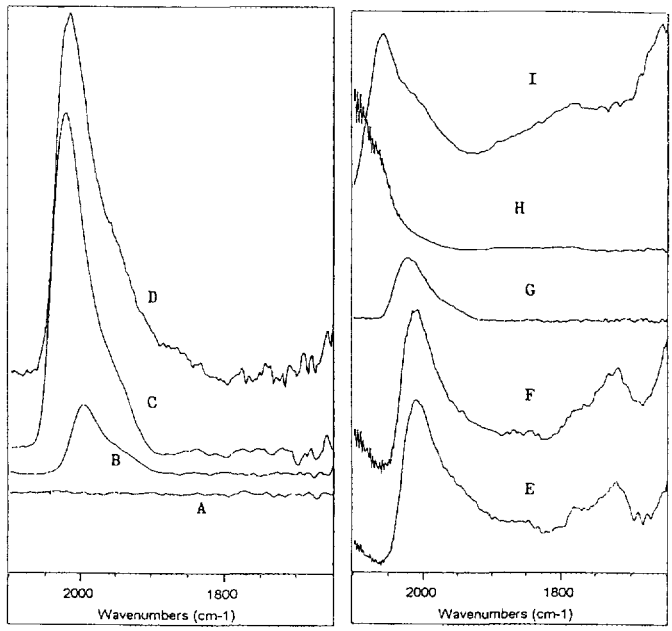

FIG. 4. Spectra recorded on the Rh/MgO sample, during experiment 9: (A) at 200°C in flowing CO_2 + CH_4, (B) at 200°C after switching from CO_2 + CH_4 to He, (C) at 300°C in flowing CO_2 + CH_4, (D) at 400°C in flowing CO_2 + CH_4, (E) at 500°C in flowing CO_2 + CH_4, (F) at 700°C in flowing CO_2 + CH_4, (G) after cooling at 50°C, (H) during a CO pulse at 50°C, (I) after the CO pulse at 50°C.

TABLE 2

Peak Maxima Detected in the Spectra Recorded during Experiment 9

T(°C)	Rh/MgO νCO (cm^{-1})	Rh/Al_2O_3 νCO (cm^{-1})	Rh/CeO_2 νCO (cm^{-1})	Ir/Al_2O_3 νCO (cm^{-1})
200	—	—	2133 (b)	2023 (b)
300	2015, 1950 (sh)	2042, 2029, 2000 (sh)	2020, 2133 (b)	2025 (b)
400	2010, 1950 (sh)	2042, 2029, 2000 (sh)	2010	2028
500	2010, 1950 (sh)	2030, 2000 (sh)	2000	2030
600	2009	2026	2000 (w,b)	2031
750	2008	2026	—	2026
50° after a CO pulse	2057	2091, 2060, 2018	2092, 2055, 2005	2057

promoted the formation of gaseous CO_2 and of cluster species with linearly bonded CO species (Fig. 4I). The formation of CO_2 indicates that reactive surface oxygen species were formed during the CO_2 reforming.

In Fig. 5 we compare the spectra collected between 100 and 500°C during experiment 9, experiment 4 (CO hydrogenation), and experiment 8 (CO_2 hydrogenation). The spectra comparisons show that bands with very similar shape and position, assigned to linearly bonded CO species, were recorded during experiments 8 and 9, while broader absorption assigned both to linear (centered near 2000 cm^{-1}) and bridged (centered near 1800 cm^{-1}) bonded CO species were detected during experiment 4. In Fig. 6 the variation of the partial pressures of the fragments with m/e = 15, 18, 28 monitored during the thermal cycle between 25 and 750°C are shown (CH_4/CO_2 = 1/1 v/v, flow rate 35 ml/min, GHSV = 70,000 h^{-1}, heating rate 60°C/min). The formation of H_2 and CO and the consumption of

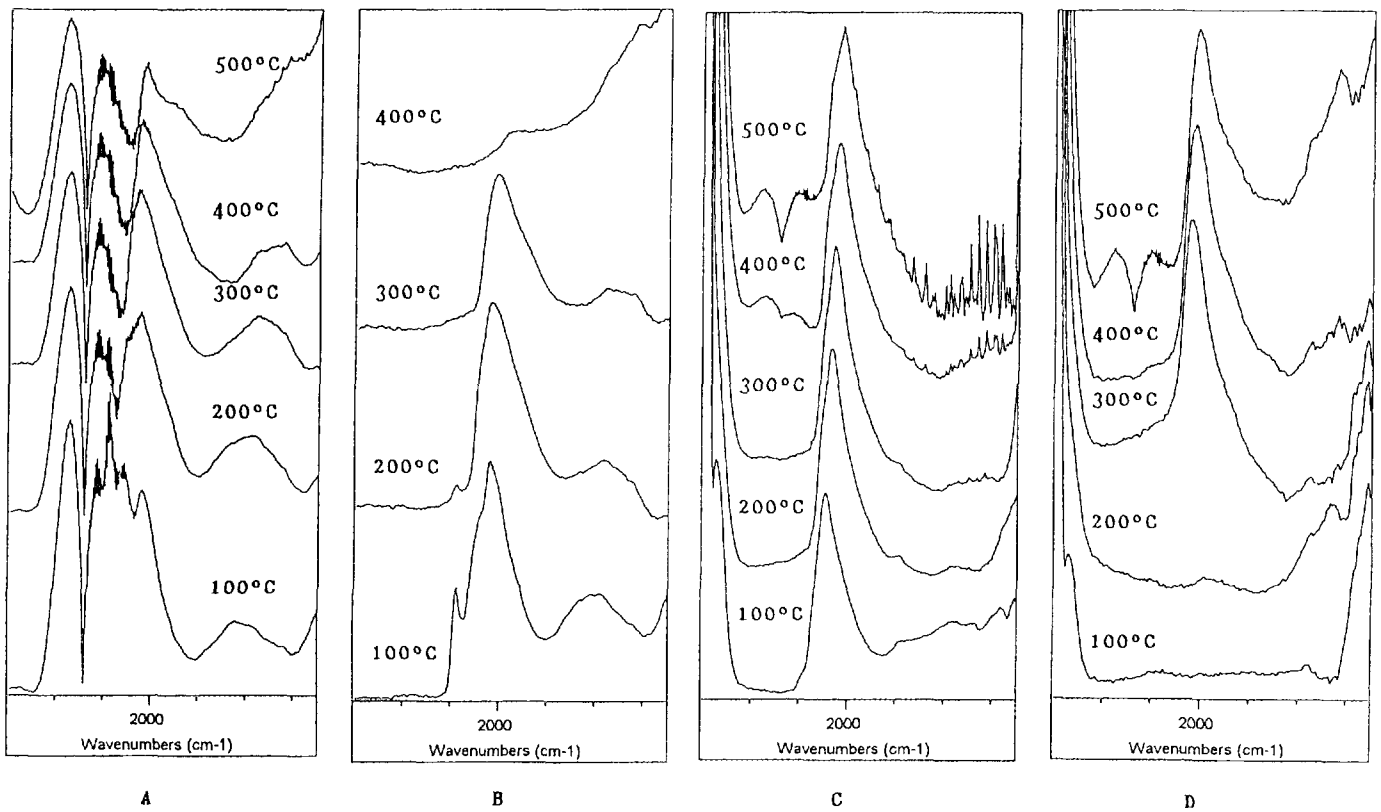

FIG. 5. Spectra of Rh/MgO recorded between 100 and 500°C during: (A) experiment 4 in flowing CO + H_2, (B) experiment 4 after switching from a CO + H_2 flow to an He flow, (C) experiment 8 in flowing CO_2 + H_2, (D) experiment 9 in flowing CO_2 + CH_4.

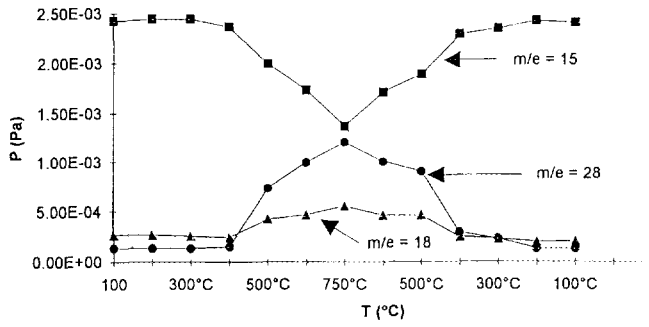

FIG. 6. Partial pressure variations of the molecular fragments of CO (m/e = 28), H_2O (m/e = 18), and CH_4 (m/e = 15) produced in the ionization chamber of the mass spectrometer during experiment 9.

CH_4 and CO_2 were detected by mass spectrometry starting from 300°C. A mass balance calculation based on the fragments partial pressure variations gave at 750°C CH_4 and CO_2 conversions of 21 and 25%, respectively (TF_{CH_4} = 0.9 s^{-1} and TF_{CO_2} = 1.1 s^{-1}). The H_2/CO ratio in the product stream was 0.88 (v/v). Conversion and TF numbers are reduced with respect to the ones achieved in the PF reactor due to the high space velocity and to the different fluidodynamic and heat transfer conditions produced in the HTHP chamber.

Rh/α-Al_2O_3. Although different Rh carbonyl clusteres were detected at the surface of α-Al_2O_3 and MgO (see Table 2 and Figs. 4 and 7), the temperature evolution of the DRIFT and mass spectra suggest that analogous phenomena are occurring at the surfaces of the two samples. Also with the Rh/α-Al_2O_3 we observed: (a) the reversible formation of carbonyl clusters at 200°C by switching the CO_2 + CH_4 flow with He (see Figs. 7B and 7C), (b) that the spectra recorded at 300 and 400°C during experiments 8 and 9 show relatively sharp bands with the same shape and position (see Fig. 8), (c) that one peak centered at 1720 cm^{-1} was formed between 400 and 750°C (Figs. 7F–7J).

A 5-min CO gaseous pulse was introduced into the cell at 50°C at the end of experiment 9. The pulse produced the formation of: (a) gaseous CO_2, (b) $Rh^I(CO)_2$ surface species, and (c) surface clusters with CO ligands in linear position (see Figs. 9N—9O). The CH_4 and CO_2 conversions measured at 750°C were 51 and 54%, respectively (TF_{CH_4} = 2.3 s^{-1}, TF_{CO_2} = 2.4 s^{-1}).

Rh/CeO_2. Carbonyl stretching bands were initially detected at 300°C and at higher temperatures in a CO_2 + CH_4 flowing environment. The bands were broader and weaker than the ones detected on the Rh/MgO and Rh/α-Al_2O_3 samples (see Table 2 and Fig. 7D) and were not stabilized in a He flow. However, the formation and the intensity increase of a peak at 1720 cm^{-1} was also observed in this case between 500 and 750°C.

The comparison between the spectra reported here and the ones previously reported (which were collected during experiments 4 and 8), shows that the $Rh^I(CO)_2$ monoatomic complexes, with peaks at 2095 and 2010 cm^{-1}, are particularly stabilized in a CO + H_2 environment, while they are not formed in CO_2 + H_2 or CO_2 + CH_4 flowing streams (Figs. 9A–9D). The DRIFT spectra reported here, also show that oxidation of surface Ce atoms occurred during the CO_2 reforming process. This conclusion was reached by observing that a broad carbonyl stretching band positioned at 2133 cm^{-1} after the reductive treatment was shifted to 2145 cm^{-1} after the CO_2 reforming reaction. The bands at 2145 and 2133 cm^{-1} are respectively assigned to the CO stretching of carbonyl groups bonded to surface Ce^{+4} and Ce^{+3} atoms. The assignment is based on CO chemisorption experiments that we performed on pure CeO_2 after a reductive treatment at 500°C in H_2 flow and an oxidizing treatment at 100°C in a O_2 flow.

The CH_4 and CO_2 conversions at 750°C were, respectively, 52 and 56%, corresponding to TF_{CH_4} = 2.3 s^{-1} and TF_{CO_2} = 2.5 s^{-1}.

After cooling at 25°C a 5-min CO pulse was introduced into the reaction chamber, this caused the formation of gaseous CO_2 and $Rh^I(CO)_2$ surface species.

Ir/Al_2O_3. The carbonylation of the Ir clusters was initially detected at 100°C in both CO_2 + CH_4 and He environments. A broad band centered near 2000 cm^{-1} was formed and gradually sharpened at increasing temperature up to 600°C (Fig. 8). Its intensity was also gradually augmented, while its frequency maximum was shifted upward by about 10 cm^{-1}. Between 600 and 750°C, a broadening of the bands (the FWHW increased ≈10%), a reduction of their intensity (5% with respect to the peak intensity recorded at 600°C), and a downward shift of the peak maxima (4 cm^{-1}) were produced. At temperatures above 500°C (when a relevant amount of reactant was converted into syn-gas), a band at 1730 cm^{-1} becomes the more intense spectral feature. The band is strongly reduced during the cooling cycle and almost disappears below 300°C. At 750°C we estimated CH_4 and CO_2 conversions of 25 and 29%, respectively (TF_{CH_4} = 0.9 s^{-1} and TF_{CO_2} = 1.1 s^{-1}).

In Figs. 11A–11C multiplets due to the CO stretching vibrations produced in the DRIFT spectra at 400°C during experiments 9, 8, and 4 are compared. Each multiplet was treated with a Fourier self-deconvolution process removing the Lorenzian broadening function (58). This procedure sharpened the components of the multiplets and showed that the same bands were produced in CO_2 + H_2 and CO_2 + CH_4 flowing streams (in both cases the multiplets show peaks at 2055, 2030, 2007, and 1964 cm^{-1}) while different spectral features were produced in a CO + H_2 environment.

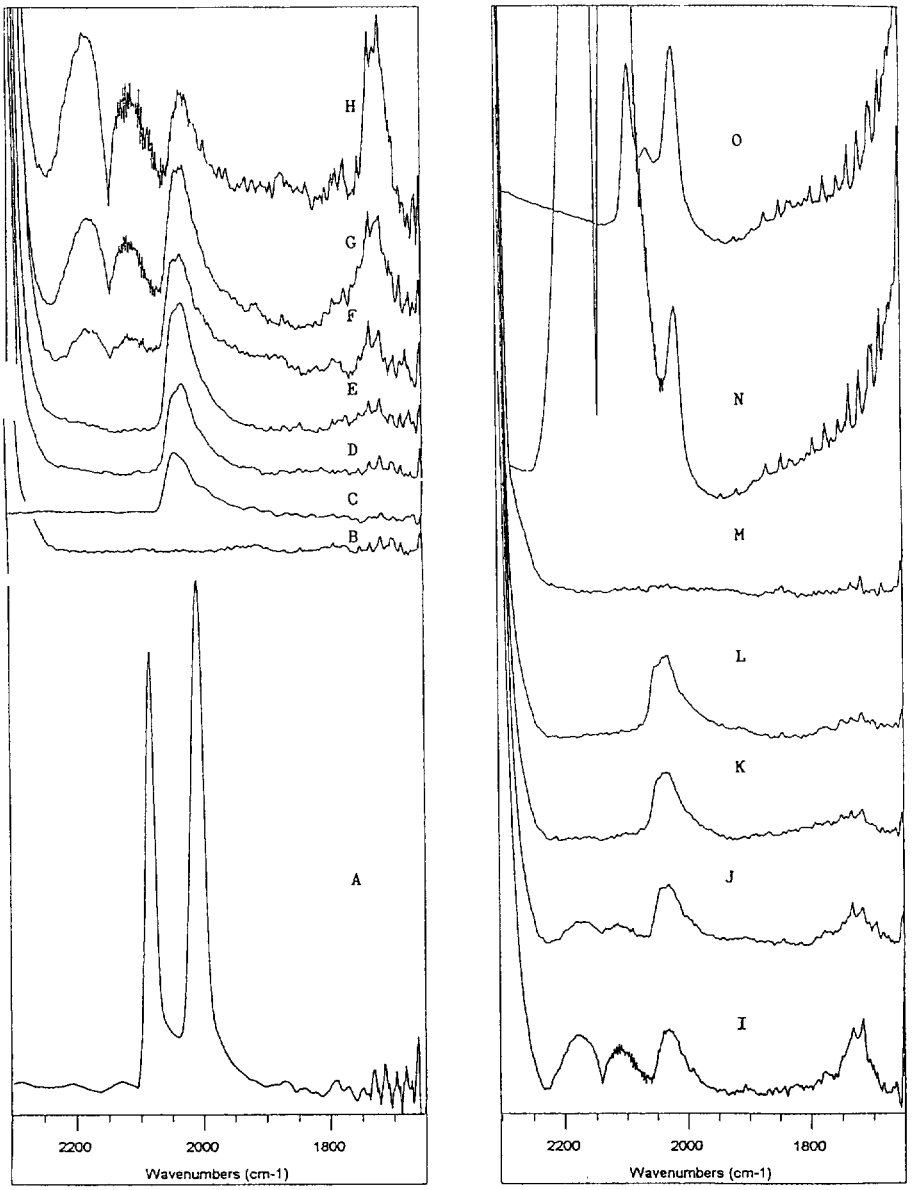

FIG. 7. Spectra of Rh/α-Al_2O_3 recorded during experiment 9: (A) freshly prepared sample, (B) at 200°C in flowing CO_2 + CH_4 atmosphere, (C) at 200°C in flowing He atmosphere, (D, E, F, G, H) at 300, 400, 500, 600, and 750°C, respectively, in flowing CO_2 + CH_4 atmosphere, (I, J, K, L, M) spectra recorded during the cooling cycle at 600, 500, 400, 300, and 200°C, respectively in flowing CO_2 + CH_4 atmosphere, (N, O) spectra recorded on the cooled sample at 25°C during and after a CO pulse in a He flow.

Experiment 10

The first two steps of this experiment (the thermal treatments in He and H_2 flows) are common to experiments 2, 4, 6, 8, and 9 and have been previously described. In the third experimental step, the samples reacted with CO_2 between 25 and 500°C. Carbonyl bands were initially detected at 50°C on Rh/MgO, and at 100°C on the Rh/α-Al_2O_3, Rh/CeO_2, and Ir/α-Al_2O_3 samples (see Table 3). The bands were sharpened and increased in intensity up to 300°C and were broadened and weakened at 500°C. At this temperature we switched from the CO_2 flow to He and cooled the HTHP cell to 25°C. The cooled samples did not show any carbonyl absorption bands. When a CH_4 flow was introduced into the cell and the temperature was increased again to 200°C, the formation of H_2 (but not of water), was detected by mass spectrometry. Rh carbonyl surface complexes were also formed between 200 and 300°C, while Ir carbonyl complexes were formed at 300 and 400°C (see Fig. 12 and Table 3). The carbonyl species

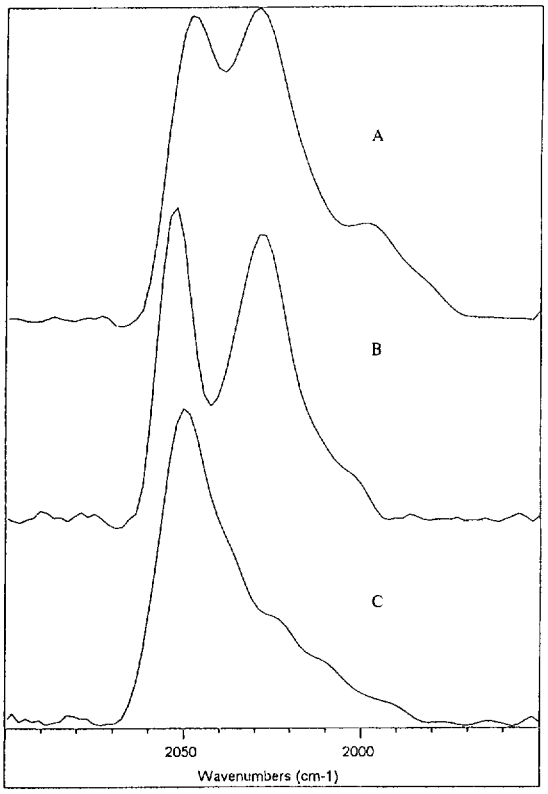

FIG. 8. Deconvolved spectra recorded at 400°C on the Rh/α-Al_2O_3 sample: (A) in flowing CO_2 + CH_4 atmosphere during experiment 9, (B) in flowing CO_2 + H_2 atmosphere during experiment 8, (C) in flowing CO + H_2 during experiment 4.

were no longer detected at 500°C, while the decomposition of methane into H_2 and surface carbon was still occurring. The mass spectrometric analysis performed during the heating steps in flowing CH_4 revealed the formation of CO and H_2 peaks (see Fig. 13).

Experiment 10 was also performed on the Ni/α-Al_2O_3 sample; in this case no surface carbonyl species and no gaseous CO were detected by DRIFT spectroscopy and mass spectrometry. The decomposition of CH_4 occurred starting from 230°C and produced gaseous H_2, a small amount of H_2O, and surface carbon.

DISCUSSION

Some of the conclusions previously obtained with experiments 1–8 (42, 43) are relevant in the discussion of the experiments 9 and 10 and are briefly mentioned. The DRIFT spectra collected during experiments 1–4 showed that, during the CO hydrogenation reactions, many different clusters with broad absorption bands assigned both to linear and bridged bonded CO species were unselectively formed. The monometallic $Rh^I(CO)_2$ species were also selectively stabilized below 300°C in an H_2 + CO flowing environment only at the surface of CeO_2. The results of experiments 5–8 showed that during the CO_2 dissociative chemisorption reactions and the CO_2 hydrogenation reactions oxidic species and a few kinds of surface carbonyl clusters were formed. The oxidic species were detected because of their ability to oxidize gaseous pulses of CO into CO_2 at 25°C. The involvement of H surface atoms which assisted in the breaking of one of the C–O bonds of the CO_2 (59) and the formation of hydrido-carbonyl clusters, was also inferred by observing that: (a) the formation of carbonyl clusters was enhanced after a reductive treatment in a H_2 flow or if CO_2 and H_2 were contemporaneously present in the reaction chamber, (b) the replacement of H_2 with D_2 in the reaction environments caused a downward frequency shift of the CO stretching.

In this work we have gained further indications of the reactivity of the oxidic species produced during the high-temperature interactions with CO_2. In experiment 10, these oxidic species reacted with CH_4 between 200 and 400°C (depending on the samples), producing both gaseous H_2 and CO pulses and carbonyl clusters (see Figs. 12A–12D, Fig. 13, and Table 3). To further clarify that the interaction with CO_2 enhanced the capability of the solid surfaces to oxidize CH_4 into CO, we also studied the CH_4 surface decomposition reactions using samples which were not previously heated in CO_2 atmosphere. In this case we observed that carbonyl clusters were formed only at the surface of the Rh/α-Al_2O_3 and Rh/CeO_2 sample. These clusters showed IR absorption features different from the ones revealed after the thermal treatment in CO_2 flowing environment. Further experiments on the reactivity of the surface oxidic species with gaseous CH_4 are in progress (experiments 11–14 of Fig. 1).

Another result reported here is the observation that similar and in some cases the same (Rh/α-Al_2O_3 and Ir/Al_2O_3) carbonyl clusters are formed during the CO_2 hydrogenation reaction and the CO_2 reforming reaction (Figs. 8A, 8B, 11A, and 11B).

Based on these findings we introduce a reaction mechanism (see Fig. 14A) for the CO_2 reform, in which CO groups are generated through two kind of reactions: (a) the breaking of one of the CO_2 bonds assisted by surface H atoms and (b) the reaction between surface oxidic species and carbidic species originating from the dissociative chemisorption of CO_2 and CH_4, respectively. We consider the clusters formed from hydrogen-assisted CO_2 chemisorption as the ones responsible for the absorption detected in the DRIFT spectra recorded during the occurrence of CO_2 reform.

This is inferred by observing that the spectra of the clusters produced through the reaction between the surface oxidic species and gaseous CH_4 (experiment 10) were different from ones recorded during the CO_2 reforming (see Figs. 4, 7, 9, 10, and 12). The same absorption bands were

TABLE 3

Peak Maxima Recorded during Experiment 10

T(°C)	Rh/MgO νCO (cm^{-1})	Rh/Al_2O_3 νCO (cm^{-1})	Rh/CeO_2 νCO (cm^{-1})	Ir/Al_2O_3 νCO (cm^{-1})
Treatments in CO_2				
50	2025	—	—	—
100	2030	—	—	—
200	2024	2050, 2030	2015	—
300	2020	2040	2000	2032, 1970 (sh)
400	2010	2030	1990	2029, 1969 (sh)
500	1985	—	1980	2024, 1971 (sh)
Treatments in CH_4				
50	—	—	—	—
100		—	—	—
200	2060, 1943	2020	2024	—
300	2060, 1943	2042, 2030	2033	2055
400	—	—	2020 (bw)	2036
500	—	—	—	—

detected during both the CO_2 hydrogenation (when the bands could be assigned to hydridocarbonyl clusters) and the CO_2 reforming reactions (see Figs. 8A and 8B).

We propose that the formation of oxygen-containing species from the dissociation of CO_2 and their affinity for the carbon atom of CH_4 is responsible for the inhibition of the carbon formation reactions [4]. We also suggest that these effects should be particularly enhanced on the CeO_2 support which is known to have oxidative properties and a good capability for oxygen storage reactions. Indeed, as described in Results, the Rh/CeO_2 sample did not show any deactivation phenomena during the 100-h reactivity test performed in the PFR.

A general observation, which follows from the achieved results, concerns the easy aggregation and disaggregation of surface cluster species under the effect of temperature and gaseous environment composition. An experimental finding, representative of these effects, is the reversible formation and decomposition of carbonyl clusters in flowing He and CO_2 + CH_4 environments, observed at 200°C (see Figs. 4A, 4B, 5B, and 5C). We tentatively propose that the phenomena (produced on the Rh/MgO and

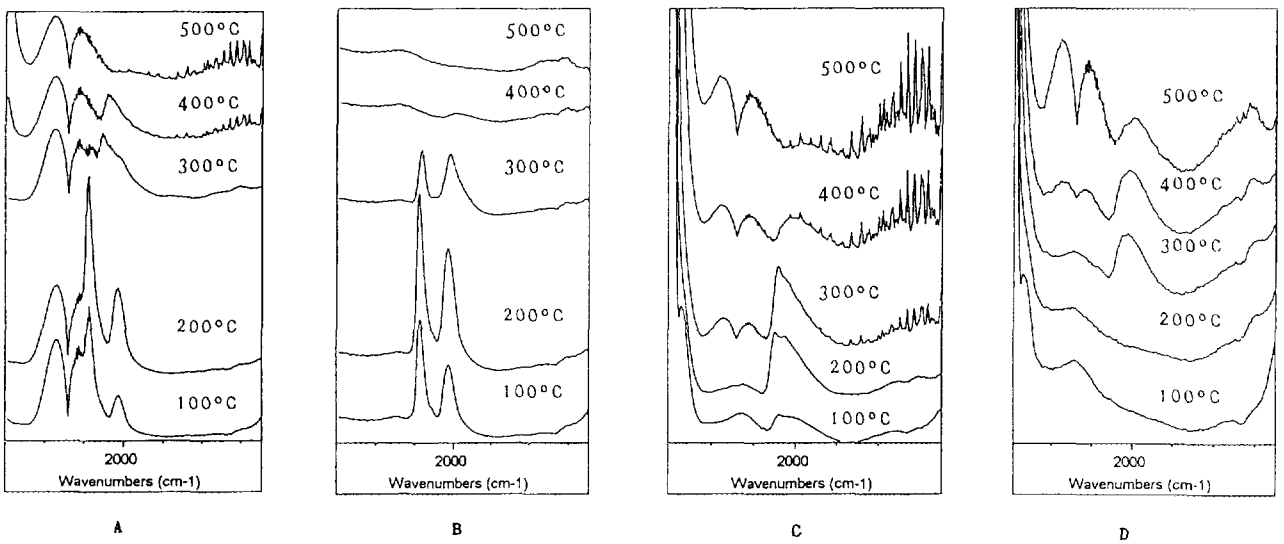

FIG. 9. Spectra recorded during the thermal cycles of experiments 4, 8, and 9 on the Rh/CeO_2 sample: (A) spectra recorded in CO + H_2 flow during experiment 4, (B) spectra recorded after switching the CO + H_2 flow with He during experiment 4, (C) spectra recorded in CO_2 + H_2 flow during experiment 8, (D) spectra recorded in CO_2 + CH_4 flow during experiment 9.

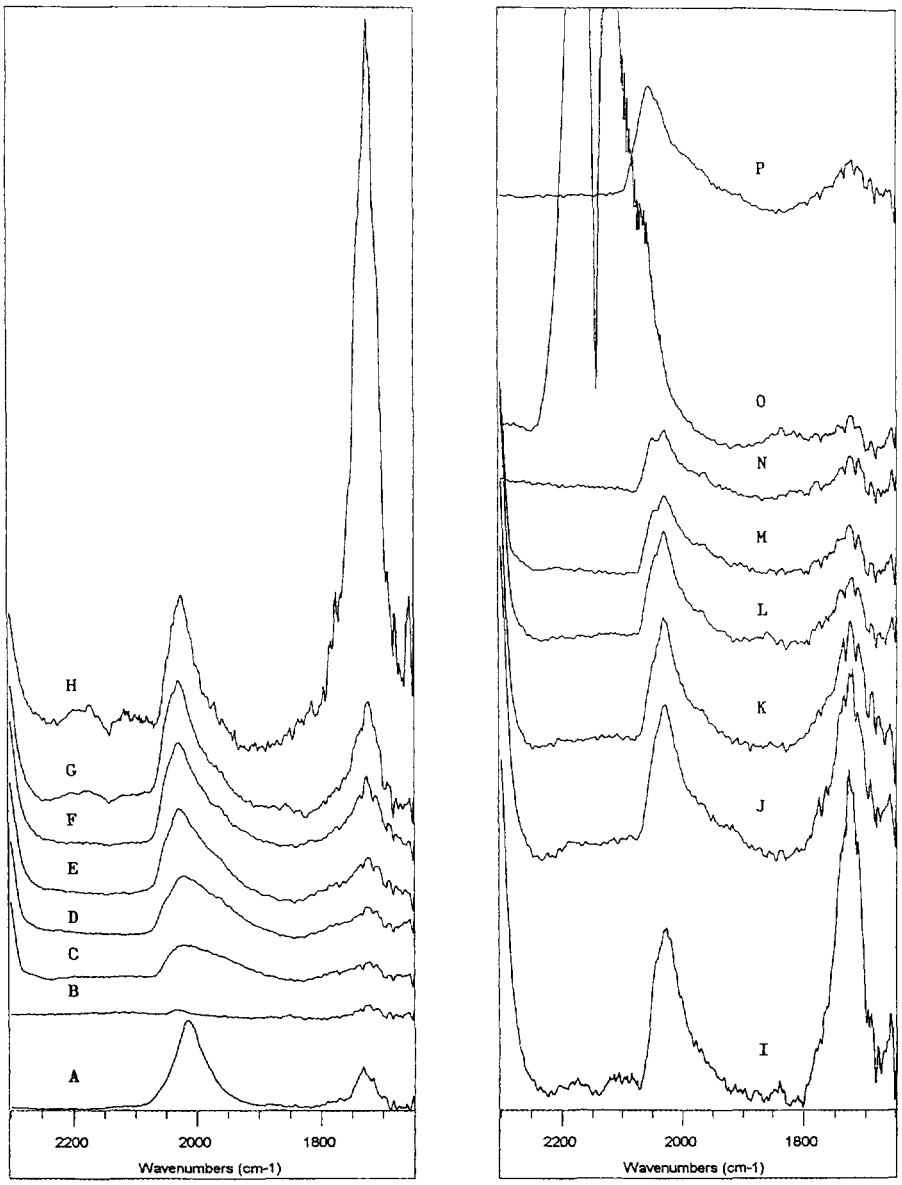

FIG. 10. Spectra recorded on the Ir/Al_2O_3 sample during the third step of experiment 9: (A) spectrum of the freshly prepared sample, (B) spectrum recorded in He flow at 25°C after the thermal treatments in He and H_2 flows, (C, D, E, F, G, H) spectra recorded in $CO_2 + CH_4$ flow during the heating cycle at 100, 200, 300, 400, 600, and 750°C, respectively, (I, J, K, L, M) spectra recorded during the cooling cycle in flowing $CO_2 + CH_4$ at 600, 500, 400, 300, and 200°C, respectively, (N) spectrum recorded in flowing He after cooling at 50°C, (O) spectrum recorded at 50°C during a CO pulse, (P) spectrum recorded in He flow at 50°C after the CO pulse.

$Rh/\alpha\text{-}Al_2O_3$) is a consequence of a delicate balance between temperature-induced reductive reactions and CO_2-induced oxidative reactions in which Rh oxygen adducts [Rh–(O_x)], Rh carbonyl clusters [Rh–CO], and bare Rh clusters [Rh_x] are interconverted according to the scheme in Fig. 14B (where [O_s] represents an atomic oxygen surface species). We point out that analogous completely reversible effects were also more sharply produced in a wider temperature range during experiments 5, 6, and 7 when the CO_2 stream was alternated with He.

The same reversible reactivity features, interpreted as a balance between aggregative and disaggregative reactions, were never observed at the surface of CeO_2. Nor were they observed on the other supports if H_2 and CO_2 were simultaneously flowed in the reaction chamber. We hypothesize that in the first case the surface of CeO_2 stabilizes oxidic species, while in the second case the presence of a large amount of hydrogen should stabilize the carbonyl clusters.

The differences and similarities between the spectra re-

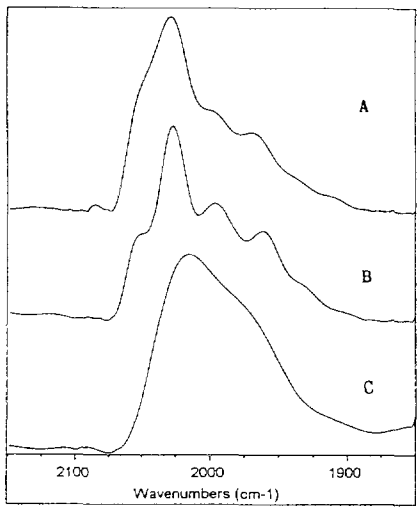

FIG. 11. Deconvolved spectra, recorded on the Ir/Al_2O_3 sample at 400°C: (A) in flowing $CO_2 + CH_4$ atmosphere, (B) in flowing $CO_2 + H_2$ atmosphere, (C) in flowing $CO + H_2$ atmosphere.

corded during CO hydrogenation, CO_2 hydrogenation, and CO_2 reform (experiments 4, 8, and 9) and quantitative catalytic tests performed in the quartz PF reactor also suggest another point of discussion.

Although the equilibrium conditions were not closely

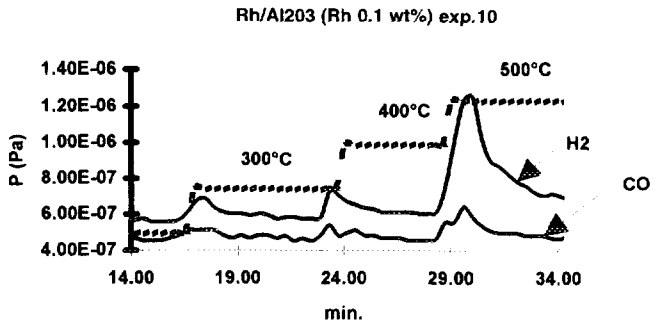

FIG. 13. Partial pressure variations with temperature and time of the fragments m/e = 28 (CO) and m/e = 2 (H_2) originated during the CH_4 decomposition on Rh/Al_2O_3. Experiment 10, fourth step.

approached in the HTHP chamber (as occurred in the PF reactor for the CO_2 reforming), conversions between 15 and 55% were achieved depending on the sample and the reaction temperature. In addition the occurrence of the WGS, reaction [5] was clearly detected during each of the three experiments (see also (53 and 54)) above 300°C. This reaction partially homogenize the composition of the reaction environments. In fact from the thermodynamic point of view, each equation representing the CO_2 hydrogenation [7], the CO hydrogenation [8], and the CO_2 reform [2], can be expressed as a linear combination of one of the remaining two with the WGS reaction [5].

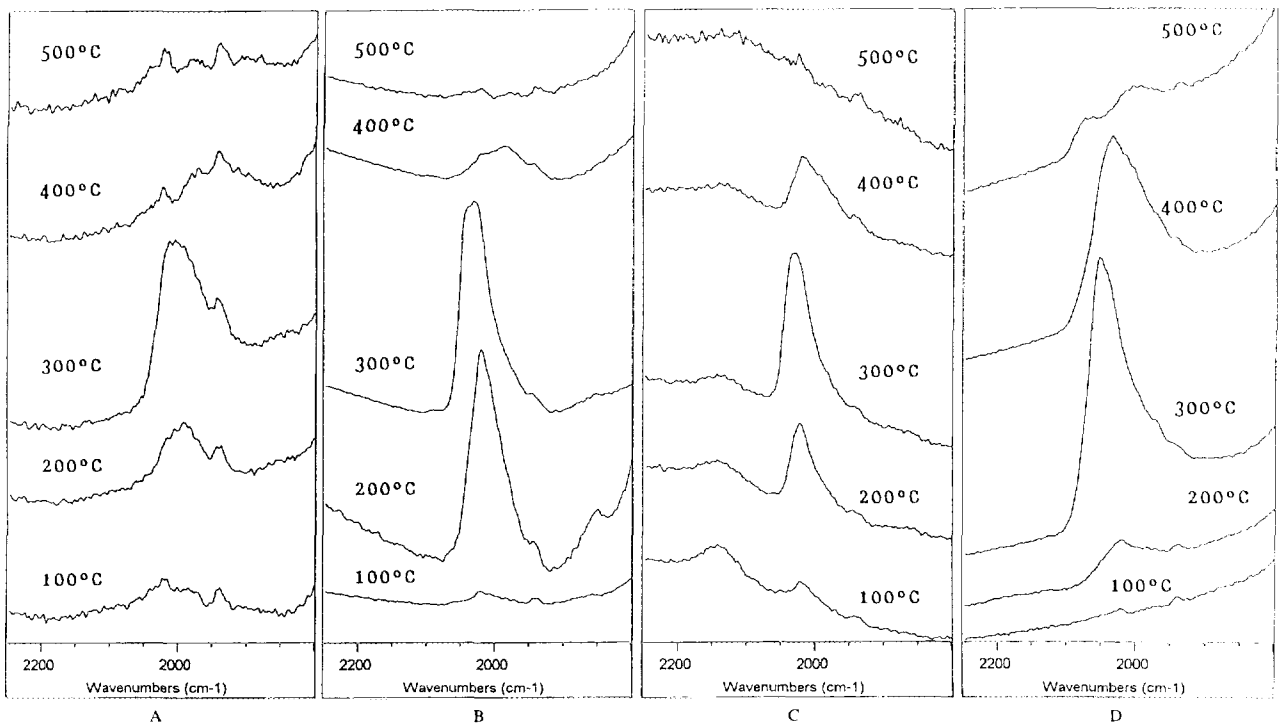

FIG. 12. Spectra recorded in flowing CH_4 stream during the fourth step of experiment 10: (A) Rh/MgO sample, (B) Rh/Al_2O_3 sample, (C) Rh/CeO_2 sample, (D) Ir/Al_2O_3 sample.

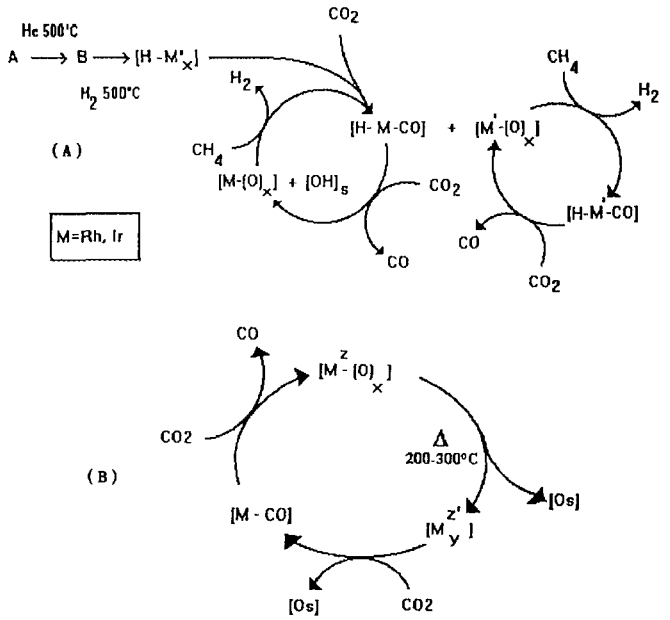

FIG. 14. (A) Scheme of the proposed mechanism for the CO_2 reforming reaction, (B) scheme of a reaction cycle proposed to account for the reversible formation and decomposition of carbonyl clusters, respectively, in He and CO_2 + CH_4 flowing environments, observed at 200°C during experiment 9.

$$CO_2 + CH_4 \rightarrow CO + 2\,H_2 \qquad \Delta H^\circ_{298\,K} = 247\ \text{kJ/mole} \qquad [2]$$

$$CO_2 + 4\,H_2 \rightarrow CH_4 + 2\,H_2O \qquad \Delta H^\circ_{298\,K} = -164.9\ \text{kJ/mole} \qquad [7]$$

$$CO + 3\,H_2 \rightarrow CH_4 + H_2O \qquad \Delta H^\circ_{298\,K} = -205.9\ \text{kJ/mole} \qquad [8]$$

$$CO + H_2O \rightarrow CO_2 + H_2 \qquad \Delta H^\circ_{298\,K} = -41.2\ \text{kJ/mole} \qquad [5]$$

For instance, Eq. [10] = −(2 × Eq. [5] + Eq. [2]) or Eq. [10] = (Eq. [11] − Eq. [5]).

However the same surface clusters were selectively produced at the same high temperatures ($T > 300$°C) only during the CO_2 hydrogenation and CO_2 reform, while during CO hydrogenation the unselective formation of many surface species was revealed. Discussing the mechanism of the CO_2-reforming reactions, we observed that the structure and the reactivity of the small surface clusters are continuously modified during each elementary step which alternatively produced reductive-aggregation reactions and oxidative-disaggregation reactions. It is the combination of these elementary steps that periodically regenerates the initial conditions. The same cycles and the same surface species are not produced by using CO and H_2 reactant mixtures because strongly chemisorbed CO and the absence, in the initial stages of the reactions, of an oxidizing agent such as CO_2, favors the unselective formation of relatively large metal aggregates and inhibits their further evolution towards small cluster species. Then some of the reactions which participate in the generation and propagation of the catalytic cycles should be irreversible in nature. These considerations agree with the results reported in the literature by other authors and by us, which indicated that, for Rh based catalysts: (a) the CO_2 hydrogenation has a selectivity and a rate for CH_4 production an order of magnitude higher than those of the CO hydrogenation reaction (67–69); (b) the CO hydrogenation is inversely proportional to the CO partial pressure (70–73), while the CO_2 methanation is positively proportional to the CO_2 partial pressure (74–76); and (c) the carbonyl complex formation is weakly affected by the presence of H_2 in the CO-containing atmosphere at temperatures up to 200°C, while it has a relevant role in the carbonyl cluster formation in the CO_2-containing atmospheres.

SUMMARY AND CONCLUSIONS

High overall TF values and high reactant conversions, close to the equilibrium values for the CO_2-reforming and water–gas shift reactions, have been achieved in a wide temperature range, between 300–750°C with Rh-, Ru-, and Ir-based catalysts under conditions in which Ni-based catalysts have been deactivated due to the carbon formation reactions.

The molecular aspects of the surface chemistry of Rh and Ir clusters during the CO_2 reforming reaction have been discussed and related to the chemistry of the CO and CO_2 hydrogenation reactions. Molecular spectra have been achieved which indicate that the same surface complexes can be produced both during CO_2 reforming and CO_2 hydrogenation reactions. The shape, position and intensity of the IR bands and their variations during thermal cycles between 25 and 750°C suggest that the selective formation of a few kinds of hydridocarbonyl clusters is achieved.

Experiments in which the interactions with H_2, CO_2, and CH_4 have been studied in separate steps, have indicated that CO_2 can be partially dissociated under the reaction conditions producing both oxidic species and carbonyl species. This reactivity is assisted by surface H atoms produced by dissociative H_2 or CH_4 chemisorption. A reaction mechanism for the CO_2-reforming reactions is proposed. The reactivity of two kinds of noble metal species, a hydridocarbonyl and an oxidic, which are periodically converted one into the other, is considered to be at the center of the catalytic cycle. The high oxidative properties of the noble metal–oxygen adducts are considered responsible for the inhibition of the carbon growth reactions.

By discussing and comparing the molecular aspects of

the reaction mechanisms of CO hydrogenation, CO_2 hydrogenation, and CO_2 reforming, we propose that the same catalytic cycles cannot be generated at the same temperature and pressure conditions (even if the reaction environment contains meaningful concentrations of the same gaseous species) if the initial reactant mixture does not contain CO_2, which has the role of inhibiting the unselective formation of large metal aggregates.

ACKNOWLEDGMENTS

We thank Prof. A. Zecchina and Prof. G. Spoto for helpful discussions and suggestions and for the careful HRTEM images, and C. Flego for the chemisorption measurements.

REFERENCES

1. Fox III, J. M., *Catal. Rev. Sci. Eng.* **35,** 169–212 (1993).
2. Rostrup-Nielsen, J. R., *in* "Catalysis Science and Technology" (J. R. Anderson and M. Boudart, Eds.), Vol. 5, pp. 1–118. Springer-Verlag, Berlin/New York/Tokyo, 984.
3. Rodler, D. E., and Twigg, M. W., "Catalysts Handbook" (M. V. Twigg, Ed.), 2nd ed., p. 1. Wolfe, London, 1989.
4. Solbakken, A., *in* "Studies in Surface Science and Catalysis" (A. Holmen, K.-J. Jens, S. Kolboe, Eds.), Vol. 61, pp. 447–455. 1991.
5. Rostrup-Nielsen, J. R., *Catal. Today* **18,** 305 (1993).
6. "Ullman's Enciclopedia of Industrial Chemistry" (B. Elvers, S. Hawkins, M. Ravenscroft, J. F. Rounsaville, and G. Schulz, Eds.), pp. 186–214. VCH, Weinheim/Basel/Cambridge/New York, 1989.
7. Ashcroft, A. T., Cheetham, A. K., Foord, J. S., Green, M. L. H., Grey, C. P. Murell, A. J., and Vernon, P. D. F., *Nature* **344,** 319–321 (1990).
8. Dissanayake, D., Rosynek, M. P., Kharas, K. C. C., and Lunsford, J., *J. Catal.* **132,** 117–127 (1991).
9. Hickman, D. A., and Schmidt, L. D., *J. Catal.* **138,** 267 (1992).
10. Hickman, D. A., Haupfear, E. A., and Schmidt, L. D., *Catal. Lett.* **17,** 223 (1993).
11. Torniainen, P. M., Chu, X., and Schmidt, L. D., *J. Catal.* **146,** 1 (1994).
12. Bharadwaj, S. S., and Schmidt, L. D., *J. Catal.* **146,** 11 (1994).
13. Hickman, D. A., and Schmidt, L. D., *Science* **259,** 343 (1993).
14. Choudhary, V. R., Mamman, A. S., and Sansare, S. D., *Angew. Chem. Int. Ed. Engl.* **9,** 31 (1992).
15. Aschcroft, A. T., Cheetham, A. K., Green, M. L. H., and Vernon, P. D. F., *Nature* **352,** 225 (1991).
16. Vernon, P. D. F., Green, M. L. H., Chetham, A. K., and Ashcroft, A. T., *Catal. Today* **13,** 417 (1992).
17. Choudhary, V. R., Rajput, A. M., and Rane, V. H., *J. Phys. Chem.* **96,** 8686 (1992).
18. Choudhary, V. R., Sansare, S. D., and Mamman, A. S., *Appl. Catal. A. Gen.* **90,** L1 (1992).
19. Hochmuth, J. K., *Appl. Catal. B Environ.* **1,** 89 (1992).
20. Lapszewicz, J. A., and Jiang, X.-Z., "Investigation of the Mechanisms of Partial Oxidation of Methane to Synthesis Gas," communication at the Symposium on Natural Gas Upgrading II, Division of Petroleum Chemistry, Inc., Am. Chem. Soc., San Francisco Meeting, April 5–10, 1992.
21. Oh, S. H., Mitchell, P. J., and Siewert, R. M., *J. Catal.* **132,** 287 (1991).
22. Rostrup-Nielsen, J.-R., and Bak Hansen, J.-H., *J. Catal.* **144,** 38 (1993).
23. Rostrup-Nielsen, J.-R., *J. Catal.* **33,** 184 (1974).
24. Rostrup-Nielsen, J.-R., and Christiansen, L. J., *J. Catal.* **43,** 287 (1988).
25. Rostrup-Nielsen, J.-R., *J. Catal.* **85,** 31 (1984).
26. Rostrup-Nielsen, J.-R., *in* "Catalyst Deactivation" (C. H. Bartholomew and J. B. Butt, Eds.). Elsevier, Amsterdam, 1991.
27. Alstrup, I., *J. Catal.* **109,** 241 (1988).
28. Gadalla, A. M., and Sommer, H. E., *J. Am. Ceram. Soc.* **72,** 683 (1989).
29. Gadalla, A. M., and Bower, B., *Chem. Eng. Sci.* **43,** 3049 (1988).
30. Gadalla, A. M., and Sommer, M. E., *Chem. Eng. Sci.* **44,** 2825 (1989).
31. Solymosi, F., Kutsain, G. Y., and Erdohely, A., *Catal. Lett.* **11,** 149 (1991).
32. Erdohely, A., Cserenyi, J., and Solymosi, F., *J. Catal.* **141,** 287 (1993).
33. Nakamura, J., Aikawa, K., Sato, K., and Uchijima, T., *Catal. Lett.* **25,** 265 (1994).
34. Richardson, J. T., and Pripatyadar, S. A., *Appl. Catal.* **61,** 265 (1990).
35. Vernon, P. D. F., Green, M. L. H., Cheetham, A. K., and Ashcroft, A. T., *Catal. Today* **13,** 417 (1992).
36. Qin, D., and Lapszewicz, J., *Catal. Today* **21,** 551 (1994).
37. Tsipouriari, V. A., Efstathiou, A. M., Zhang, Z. L., and Verykios, X. E., *Catal. Today* **21,** 579 (1994).
38. Blom, R., Dahl, I. M., Slagtern, A., Sortland, B., Spjelkavik, A., and Tangstad, E., *Catal. Today* **21,** 535 (1994).
39. Toshio, U., Kimio, K., and Junji, N., JP 04,367,501.
40. Walker, R. H., and Willems, P. A., Can. Pat. Appl. CA 2,019,001.
41. Gas Research Institute, Neth. Appl. NL 90 01,508.
42. Egglestone, F., EPA 87303307.
43. Masato, O., JP 91,57,002.
44. Heck, R. M., EPA 83305887.
45. Lywood, W. J., EPA 89302539.5.
46. Kobylinski, T. P., US 5,112,527.
47. Sie, S. T., UK Pat. Appl. GB 2,249,555.
48. Fujitani, Y., and H. Muraki, US 4,087,259.
49. Heck, R. M., EPA 83305887.
50. Basini, L., Marchionna, M., Sanfilippo, D., and Rossini, S., GB 9118116.
51. Basini, L., Marchionna, M., Sanfilippo, D., and Rossini, S., GB 2240284.
52. Van Kaman, K. A., Jacobs, L. L. G., European Pat. Appl. 576,096.
53. Basini, L., Marchionna, M., and Aragno, A., *J. Phys. Chem.* **23,** 9431 (1992).
54. Basini, L., and Aragno, A., *J. Chem. Soc. Faraday Trans.* **90,** 787 (1994).
55. Bozon-Verduraz, F., and Bensalem, A., *J. Chem. Soc. Faraday Trans.* **90,** 653 (1994).
56. Hestl, G., Trian Trafillou, N. D., and Knozinger, H., *J. Phys. Chem.* **97,** 666 (1993).
57. Little, L. H., Kiselev, A. V., and Lygin, V. I., *in* "Infrared Spectra of Adsorbed Species," p. 81. Academic Press, New York, 1966.
58. Kauppinen, J. K., Moffat, D. J., Mantsch, H. H., and Cameron, D. G., *Appl. Spectrosc.* **35,** 271 (1981).
59. The results of experiments 5–8 indicated that the presence of H_2 enhanced the CO_2 chemisorption reactions and caused the production and stabilisation of hydridocarbonyl clusters, the formation of which was inferred by comparing the spectra obtained in $CO_2 + H_2$ and in $CO_2 + D_2$ gaseous mixtures (53). The observed H induced enhancement of the CO_2 chemisorption properties and was found to have many analogies with organometallic chemistry reactions (60–65) occurring through a metal-mediated interaction between the CO_2 and the hydride species producing the breaking of one of the C–O bonds of CO_2.
60. Eisemberg, R., and Hendrikson, D. E., *Adv. Catal.* **28,** 79 (1979).
61. Darensbourg, J., and Ovalles, C., *J. Am. Chem. Soc.* **106,** 3750 (1984).
62. Pugh, J., Bruce, M. R. M., and Sullivan, B. P., *Inorg. Chem.* **30,** 86 (1990).
63. Braunstein, P., Hatt, D., and Nobel, D., *Chem. Rev.* **88,** 747 (1988).
64. Darensbourg, D. J., Wiengraffe, H. P., and Wiengraffe, P. W., *J. Am. Chem. Soc.* **112,** 9252 (1990).
65. Palmer, D. A., and van Eldik, R., *Chem. Rev.* **83,** 651 (1983).

66. Darensbourg, D. J., and Kudaraski, R., *Adv. Organomet. Chem.* **22,** 129 (1993).
67. Solymosi, F., and Erdohely, A., *J. Mol. Catal.* **8,** 47 (1980).
68. Vannice, M. A., *J. Catal.* **37,** 449 (1975).
69. Bardet, R., and Trambouze, Y. C. R., *Acad. Sci. Paris Ser. C* **288,** 101 (1979).
70. Biloen, P., and Sachtler, W. H. H., *Adv. Catal.* **30,** 165 (1981).
71. Vannice, M. A., *Catal. Rev. Sci. Eng.* **14,** 153 (1976).
72. Bell, A. T., *Catal. Rev. Sci. Eng.* **23,** 203 (1981).
73. Mills, G. A., and Stefgen, F. W., *Catal. Rev. Sci. Eng.* **10,** 139 (1978).
74. Bartholomew, C. H., *Stud. Surf. Sci. Catal.* **64,** 158 (1991).
75. Solymosi, F., Erdohely, A., and Basagi, T., *J. Catal.* **68,** 371 (1981).
76. Solymosi, F., Erdohely, A., and Basagi, T., *J. Catal.* **62,** 165 (1981).